Engineering Macro-Scale, Lumenized Airway Tubes of Defined Shape via Multi-Organoid Patterning and Fusion

Ye Liu[1], Catherine Dabrowska[2,3], Antranik Mavousian[2], Bernhard Strauss[4], Fanlong Meng[5], Corrado Mazzaglia[1,6], Karim Ouaras[1,7], Callum Macintosh[1], Eugene Terentjev[8], Joo-Hyeon Lee[2,3,*], Yan Yan Shery Huang[1,8*,#].

[1]Department of Engineering, University of Cambridge, Cambridge, UK. [2]Wellcome – MRC Cambridge Stem Cell Institute, University of Cambridge, Cambridge, UK. [3]Department of Physiology, Development and Neuroscience, University of Cambridge, Cambridge, UK. [4]Department of Biochemistry, University of Cambridge, Cambridge, UK. [5]CAS Key Laboratory of Theoretical Physics, Institute of Theoretical Physics, Chinese Academy of Sciences, Beijing, China. [6]MRC Cancer Unit, University of Cambridge, Cambridge, UK. [7]The Nanoscience Centre, University of Cambridge, Cambridge, UK. [8]Cavendish Laboratory, University of Cambridge, Cambridge, UK. *Correspondence, [#]Lead contact: yysh2@cam.ac.uk

Abstract

Epithelial, stem-cell derived organoids are ideal building blocks for tissue engineering, however, scalable and shape-controlled fusion of epithelial organoids into larger and anatomical structures has yet to be achieved. Here we establish Multi-Organoid Patterning and Fusion (MOrPF) as a robust bioengineering approach to assemble individual airway organoids of different sizes into upscaled airway tubes with pre-defined shapes. Multi-Organoid Aggregates (MOAs) undergo accelerated fusion in a matrix-depleted, free-floating environment, possess a continuous lumen and maintain prescribed shapes without an exogenous scaffold interface. We show that MOrPF exhibits a well-defined three-stage process of inter-organoid surface integration, luminal material clearance and lumina connection. The observed shape stability of patterned MOAs is confirmed by theoretical modelling based on organoid morphology and the physical forces involved in organoid fusion. We further characterized MOAs with selected markers for tracheal epithelium. MOrPF enables upscaled organoid engineering to produce integrated organoid-devices and structurally complex organ tubes.

Introduction

Engineered fusion of multi-cellular materials, such as spheroids and organoids, represents a biomimetic cell assembly process fundamental to the fields of biofabrication, tissue engineering and *in vitro* tissue modelling[1,2,3]. Organization and fusion of cell aggregates to achieve prescribed shapes (and functions) depends on the selection of initial multi-cellular building blocks. Coalescence of solid-core spheroids can readily occur via so-called 'tissue liquidity'[4], in aggregates of epithelial cells[1], fibroblasts[5], mesenchymal stem cells[6], and in hybrid spheroids consisting multiple cell types[7,8]. Guided-assembly through micro-fabricated molds or 3D-printing can further define the three-dimensional (3D) architecture of fused tissue constructs[9]. In the last decade, organoids have emerged as a powerful tool to study the behavior of their tissue of origin[10,11,12]. Given their close resemblance to native organs in histology and cell composition, organoids represent ideal modular units for the biofabrication of biomimetic organs[13,14]. While fusion has been demonstrated in pairs of brain organoids[15,16] and in collagen-embedded intestinal organoids[17], upscaled fusion of cystic epithelial organoids into shape-controllable, large lumenized tissues remains challenging. In order to produce functional epithelial tubes mimicking biological tubes with an elongated lumen, such as the trachea, organoid fusion requires both the seamless surface integration between adjacent organoids and the inter-connection of the fluid-filled lumina. Here, using mouse tracheal epithelial organoids, we show multi-organoid patterning and fusion (MOrPF), to create lumenized macro-tubes of defined shapes. We patterned individual organoids into shape-defined multi-organoid aggregates (MOAs) and employed a free-floating environment to encourage inter-organoid surface connection and lumenization. Notably, the size of fused organ tubes can be prescribed to match that of an adult mouse trachea. A theoretical model is proposed to explain MOA shape maintenance post-patterning, in the absence of a solid matrix or shape-supporting scaffold interface. We envisage these macro-organoid tubes as a foundation for several emerging downstream applications, including organoid-microfluidics integration and multi-tissue organ reconstruction.

Results

MOAs undergo a three-stage fusion process leading to lumenized tube formation

Starting with individual airway organoids derived from adult mouse tracheal epithelial cells, we established a robust organoid fusion platform, for the upscaled engineering of size-relevant tissue constructs (Fig. 1a-I). Isolated single tracheal basal stem cells form cystic airway organoids of heterogeneous sizes in 3D Matrigel (a mouse-derived extracellular matrix), as previously reported[18] (Supplementary Fig. 1a). Occasionally, we observed pairs of organoids fused into randomly shaped cysts (Supplementary Fig. 1b). To test whether liberating organoids from Matrigel would enhance fusion, we mechanically dissociated airway organoids from Matrigel, and cultured them in a free-floating condition (termed as Matrigel-depleted culture). Though a low amount of Matrigel could be carried over into the MOrPF process, this should not be enough to form a constraining layer around organoid aggregates. In such Matrigel-depleted condition, organoids fused more frequently and formed inter-connected lumina (Supplementary Fig. 1c,d); however, the size and shape of fused products remained highly heterogeneous. To control the final geometry of the fusion products and to improve overall fusion efficiency, we developed a multi-organoid patterning and fusion (MOrPF) workflow as shown in Figure.1a-II. Day-12 organoids were dissociated from Matrigel drops and transferred in a 3D-designed polydimethylsiloxane (PDMS) mold to form shape-patterned multi-organoid aggregates (MOAs). Depending on the PDMS template size and airway organoid diameter, approximately 100-1400 organoids were assembled in each well of the PDMS mold. Subsequently, MOAs were released from the PDMS template and cultured in the floating condition for effective fusion and lumenization.

We next quantified the overall morphological changes of MOAs during the MOrPF process, by measuring the projected area of the MOA in relation to its inner dense matter (cellular materials in the center of organoids and MOAs), across different stages of MOrPF (Fig. 1b, Supplementary Fig. 2a). Upon release from the PDMS mold, the patterned MOA retained its prescribed geometry with an opaque appearance (Day 1). An external layer of cells started to envelop the outer surface of the MOA (Day 3, envelopment), leading to the smoothening of MOA external contour by day 6. During this time, the luminal content of the MOA gradually cleared out, as quantified by the normalised projected area of inner matter, i.e. the Apparent Inner Matter Ratio (AIMR) (Fig. 1b(iii)). By Day-10, the MOA resembled a quasi-translucent, closed-end tube, which exhibited

intermittent lumen shrinkage and re-expansion (Fig. 1b(ii), (iii)). Similar epithelium rupture and inner fluid release, followed by lumen closure and re-expansion, have been observed in single epithelial organoid[19] and the mouse blastocytes[20]. Since the time required for MOA fusion increases with the increase in MOA size (Supplementary Fig. 2f), we chose AIMR, instead of days in culture, to normalize the fusion stages among MOAs of different sizes. By correlating AIMR dynamics with bright field images, we identified three critical stages during MOA fusion progression: Stage I: Envelopment and Compaction; Stage II: Lumen Clearance; and Stage III: Stabilization (Fig. 1c). These key stages were typical for patterned MOAs of a range of sizes (Supplementary Fig. 2b-d). During Stage I, MOAs acquired an outer layer of enveloping cells and underwent subsequent compaction, showing a peak AIMR value ~0.9 (Fig. 1b(iii), Supplementary Fig.2d). During Stage II (the longest stage in MOrPF), MOAs gradually cleared their luminal content, resulting in a decrease in AIMR from ~0.9 to ~0.35 (Fig.1b(iii), Supplementary Fig. 2d,e). During Stage III, stabilized MOAs developed a smooth outline and a quasi-translucent lumen, while retaining the aspect ratio prescribed by the PDMS mold (Fig.1d, e). Together, our data suggest that MOrPF is a robust process for the assembly and fusion of small, heterogeneously-sized organoids into macro-scale, shape-definable epithelial tubes.

Inter-organoid envelopment during Stage I is a pre-requisite for MOA fusion

We next investigated organoid behaviors throughout the MOA fusion process, using live imaging on small clusters of organoids cultured under different conditions. We first observed organoid aggregation and cellular bridge formation (termed ‘inter-organoid envelopment’) between touching, adjacent organoids in the floating culture (Fig. 2a(i)). After dissociation from Matrigel, those organoids were able to aggregate spontaneously; upon establishment of the inter-organoid contact, a cellular bridge started to form between the touching organoids and continued to expand into a shared envelope covering the organoids (Fig. 2a(ii), Supplementary Video 1). Within a few days, inter-organoid envelopes became visible at multiple locations of a MOA, gradually integrating into a continuous layer encasing all organoids within the aggregate (Supplementary Fig. 3a). Interestingly, organoid aggregation and envelopment was significantly reduced with increased Matrigel concentration, as supported by our comparative data on MOA fusion in Gel-suspension (Matrigel added at a 20% volume concentration in medium, Fig. 2b, Supplementary Fig. 3b) and 100% Matrigel-embedded cultures (Fig. 2c, Supplementary Fig. 3d,e). In the Gel-suspension condition, inter-organoid enveloping efficiency dropped to

below 30% (Fig.2e) and the onset of envelopment was delayed after organoids had established contact (Fig. 2b(ii)). When embedded in 100% Matrigel, organoids rarely aggregated or developed envelopes, even in close proximity (Fig. 2c-e). Without efficient envelopment, MOAs failed to develop fused lumina (Fig 2f). Fusion efficiency in MOAs (with projected area of 0.6-1 mm^2) was <20% in Gel-suspension and <10% in Matrigel-embedded culture (Fig. 2f). By contrast, in the floating condition, over 60% of organoids formed lumenized MOAs by Day 7, which further increased to over 90% by Day 11. To further explore organoid fusion possibility in the presence of a non-adherent hydrogel such as agarose, we placed organoids in a floating culture supplemented with 0.5% weight percent agarose. Organoid aggregation and envelopment were not inhibited by agarose fragments, but the lumen clearing process seemed restricted (Supplementary Fig. 3f). Together, these data suggest that after organoid dissociation from the adhesive Matrigel matrix, envelope formation is required for organoid fusion and MOA lumenization. Inter-organoid envelopment is enhanced in the floating culture, which largely liberates organoids from organoid-substrate interaction, while permitting organoid-organoid interaction.

Cellular matter release results in MOA lumen clearance

After the establishment of a shared envelope, we further observed MOA compaction and inner matter release, using live imaging with a 2-day interval, over 6 days. Coinciding with envelope extension, inter-organoid space decreased within MOAs (Fig. 3a), allowing increased interfacial contact between adjacent organoids (Supplementary Video 2). During the lumen clearing stage, MOAs developed large, connected cavities by releasing their inner contents (inner matter release, Fig. 3b(i)) from multiple epithelium rupture sites (Supplementary Video 3-4). Given that the AIMR of MOAs gradually stabilized by the end of Stage II-lumen clearance, we asked whether the local release of inner matter correlated with the ensemble-level MOA opacity. Following the local release dynamics of MOAs in their early (AIMR>0.8), mid (0.4<AIMR<0.7) and late (AIMR<0.4) lumenization phases, we found that MOAs extruded inner matter in an intermittent, ‘start and stop’ fashion (Supplementary Fig.4), which could take from a few hours to several days at one release site. We then calculated the local release speed, by quantifying the hourly increase in the projected area of a released inner cluster. As shown in Fig. 3b (ii), going from the early, to mid and late lumen clearing phases, both the mean and the maximum release speeds decreased, indicating the accomplishment of lumenization and the stabilization of

MOAs.

MOA shape stability during fusion can be explained by a theoretical model based on airway organoid morphology and physical forces

Since MOAs retain their prescribed, elongated shapes in the floating culture for weeks (Fig. 1 d, e), we postulated that such shape stability could originate from the characteristic airway organoid morphology, i.e. fluid-filled cysts enclosed by an epithelial layer (which was treated as an epithelial 'shell' in the context of the following physical model). We examined the physical forces at play during the organoid fusion process, the balance of which determines the overall shape of a fused MOA. To construct a simple mathematical model of organoid fusion and MOA shape maintenance, we consider a pair of spherical, equal-sized epithelial organoids (Fig. 3c(i)), each of overall thickness d (the pseudostratified layer of epithelial cells), filled with incompressible fluid. Before fusion, the organoids (which had grown for 12 days post-plating in Matrigel) are assumed to have a radius R_0. Observations showed that upon their contact, a stable dumbbell-like structure would form (Fig. 3 c(iii)), consisting of two spherical caps of a new radius R, and an interfacial adhesion 'disk' in between, which is flat when the two organoids were of the same radius initially. To preserve their inner volume, each organoid shell has to be stretched, which causes an elastic energy penalty[21,22] in their outer surfaces (see Supplementary Fig. 5 and Additional information for details). This energy cost, defined by the elastic modulus G of the epithelial shell, balances against the energy gain from the adhesion disk due to the favorable surface energy γ[23,24]. These two competing factors determine the shape of the fused object, before the gradual disintegration of the interfacial disk, which takes a few days to weeks. The preferred shape of the fused organoids is given by the plot of the spherical cap height h, as a function of a single control parameter: the non-dimensional ratio Gd/γ (Fig.3 c(ii)).

Taking the measured values of G = 200 Pa [21] and d = 20 μm (Fig. 4a), and the estimated adhesion energy at the initial cell-cell contact: γ = 2 mN/m, we find the control parameter $Gd/\gamma = 2$, and the predicted height: h= $0.5R_0$. The observed shape of the organoid dumbbell (Fig.3 c(iii)) is almost exactly matching this prediction of $h \sim 0.5R_0$, suggesting that our presented model based on two competing physical forces is a good description of

the initial scenario in organoid fusion.

Next, we examined how the dumbbell shape established after the initial inter-organoid envelopment can remain stable over the stages of inner matter release and lumen interconnection. Organoid shell rupture can result in fluid release, and consequently, the release of the weakly bound inner matter material. Such release events equilibrate the external and internal fluid pressure, when the inner matter release stops. Another plausible pressure equilibration event could arise from the cellular plastic flow adjusting the area of the shell. With this auto-pressure regulation, the inner fluid pressure would not accumulate excessively even after the disintegration of the interfacial disk. This physical insight could explain the intermittent nature of inner matter release patterns (Supplementary Fig. 4). After the period of plastic flow (hours to days) of cells on the outer shell of the fused organoids, the elastic tension will be released, and the internal pressure remains equilibrated. The new dumbbell shape will become the new quasi-equilibrium state, maintained by the high bending rigidity of the shell (see the estimate in Additional Information) even after the disintegration of the adhesion disk (days to weeks, Fig.3d). Such elongated shape was thus maintained throughout MOrPF, after MOAs being prescribed by the initial patterning process.

Biological characterization of fused MOA tubes

We next assessed the cellular morphology and epithelial composition of MOAs at different stages of the MOrPF process. At Stage I-envelopment and compaction, Hematoxylin and Eosin (H&E) staining revealed that the development of the MOA enveloping cell layer was contributed from the outer epithelial layers of individual organoids positioned near the MOA surface (Fig. 4a). Proceeding to Stage II-lumen clearance, individual organoids were mostly unidentifiable, and the contour of MOAs became smooth and continuous. In the MOA center, lumina appeared inter-connected though some interfacial discs remained. Finally, in Stage III-stabilization, a continuous lumen developed in MOAs. Immuno-histochemistry staining for airway epithelial markers showed long-term maintenance of airway basal stem cells expressing p63 and Keratin-5 (Krt5) in MOAs up until, and including, Stage III-stabilization (Fig. 4b, Supplementary Fig. 6a). Differentiated ciliated cells expressing acetylated tubulin (ACT) were observed in Stage II MOAs (Fig. 4c). However, we observed the gradual loss of differentiated luminal cells expressing Keratin-8 (Krt8), and an increased disorganization of

the typical pseudostratified airway epithelium over the fusion process (Fig. 4b, Supplementary Fig. 6a). To better understand the cellular processes responsible for inter-organoid interactions, we examined key polarity markers during fusion. Whereas unfused organoids displayed intact apical-basal polarization, with the basal membrane expressing fibronectin, the apical junction expressing ZO-1, and the lateral membrane expressing E-cadherin, MOAs revealed disorganized polarization (Supplementary Fig. 6b,c). Epithelial cells of stabilized MOAs had reversed polarization, with fibronectin marking the cellular surfaces facing the central lumen. Furthermore, although epithelial cells in the MOAs maintained expression of E-cadherin, expression of ZO-1 was significantly decreased. Our data collectively suggest that upon Matrigel depletion and organoid fusion in the floating condition, fused MOA tubes retain a single epithelial layer of basal cell identity without pseudostratified epithelial morphology, and showed marked changes in epithelial polarity. This is possibly due to the reduction of extra-cellular matrix (ECM) proteins after Matrigel depletion at the outside of MOAs[25].

Downstream processing of MOAs for tissue engineering applications

Since the MOrPF process creates fused airway MOA tubes in a highly efficient (>90% fusion success rate, Supplementary Fig.1d) and shape-controllable manner, it opens up possibilities for scalable organoid-device integration, multi-tissue interaction, and organ architecture reconstruction. For example, fluid transport is characteristic of many organs and plays an important role in epithelium development and function[26,27]. Our engineered airway MOA tubes, of a size similar to the mouse trachea (1-1.5 mm inner diameter[28]), were perfusable and exhibited cyclic lumen expansion and relaxation, in synchronization with a peristaltic input flow of culture medium (Fig. 4d(i), Supplementary Video 5). Such a flow-able system (Supplementary Fig.7a,b) shows potential for studying epithelial mechanics, as well as for drug testing and disease modelling[29]. It is also an initial step for designing a fluidic system for larger organ tubes, where the lumen is accessible within a closed, controllable system separated from the environment on the basal side. Additionally, given that most organ epithelia including trachea epithelium are supported by mesenchymal tissues such as smooth muscle cells (SMCs) and basement membrane, we further engineered a SMC support for fused airway MOA tubes, by co-culturing them with mouse vascular aortic smooth muscle cells (MOVAS). A substrate-detachable SMC sheet was obtained using a temperature-responsive plate, and carefully wrapped around a fused airway MOA tube to create an integrated tissue (Fig. 4d(II)). This co-culture example illustrates the flexible adaptability of our

engineered epithelial tubes for the biofabrication of complex, multi-tissue organ analogues. Finally, we demonstrated that MOA modular units can be connected to each other and jointly fused into macroscopic, bifurcating tubes, mimicking the branching architecture in many epithelial organs (Fig. 4d(III)). The feasibility of fusing mouse intestinal organoids into 4 mm-long intestinal tubes in our floating system revealed the broader application of MOrPF across other types of epithelial organoids (Supplementary Fig.7c).

Discussion

Classical bio-assembly processes largely rely on solid hydrogel matrices[30,31,32] or patterned scaffolds[5] to both define and maintain the architecture of engineered tissues. Recent work demonstrated that a suspension culture, in place of solid matrices, improves the homogeneity and throughput of individual organoid culture[33]; however, the sequential self-organizing cellular events remained unexplored. Here we expand the potential of the floating culture within an organoid-assembly workflow, by developing the MOrPF process that fused individual, heterogeneous organoids into tissue-scale epithelial tubes of defined geometry. Such efficient organoid fusion is realized in a Matrigel-depleted, free-floating system that harnesses the self-organization capacity of organoids. Importantly, we discovered two critical fusion steps in MOA fusion and lumenization: inter-organoid surface integration and subsequent inner matter release. Interestingly, our findings showed great morphological similarities to selected *in vivo* epithelial tubulogenesis[34]. The establishment of inter-organoid envelopes in MOrPF mirrors the formation of protrusion-like fusion fronts between adjacent tubular branches in the embryonic *Drosophila* trachea[35] and chicken lung[34]. Moreover, the release of inner cell matter from MOAs may resemble cavitation (elimination of redundant cells from a solid-core tissue) in the developing *Drosophila* wing[36] and mouse salivary gland[37]. It would be of interest to further investigate the mechanisms of inter-organoid adhesion and cell migration[38] during envelopment, and the possible involvement of apoptosis[36,39] during inner cell deposition and release. Moreover, our study suggests an alternative design pathway for epithelial organoid engineering, in which shape-patterning via molding is required only at the initial organoid assembly stage, while the prescribed geometry can be retained long-term in the floating culture. This is in stark contrast to existing strategies of constructing tubular epithelial structures, which rely on exogenous shape-supporting matrices or scaffolds[17,40]. Theoretical modelling suggests that the long-term shape stability of

patterned MOAs originates from the biomechanical properties of fluid-filled epithelial organoid cysts. This also makes the fusion mechanism of cystic organoids distinct from that of solid-core spheroids, in which shape-maintenance is either transient (days), or requires a bounding scaffold or matrix[1,4,5]. Our engineered epithelial tubes using the MOrPF process are reproducible in geometry, readily accessible for further co-culture or matrix integration, and compatible with fluidic techniques to enable lumen access and fluid transport. We envisage that such macroscopic tubular epithelial building blocks could have broad implications in creating size-relevant, structurally complex, multi-tissue organ mimics[14].

Methods

Generation and culture of mouse airway organoids

Mouse airway organoids were generated following a published protocol[41]. Briefly, trachea was dissected from 7-13 weeks old mice, and incubated in 50 U/mL dispase (Sigma) for 45 minutes (37°C). 10 mL PBS was flushed through the trachea using a syringe needle to release the trachea epithelium. Extracted cell sheets were incubated in trypsin for 5 minutes (37 °C) and dissociated single cells were mixed with growth factor-reduced Matrigel (Corning) on ice to a concentration of 1 x 10^5 cells/mL. 30 µL dropets of Matrigel-cell mixture was plated in a 48-well plate and left in incubator for 15 minutes (37°C) for gelation. Matrigel droplets were topped with 250 µL DMEM-Ham's F-12 media supplemented with 0.5 mg/mL penicillin-streptomycin, 10 µg/mL insulin, 5 µg/mL transferrin, 0.1 µg/mL cholera toxin, 25 ng/mL EGF, 30 µg/mL bovine pituitary extract, 5% FBS and 0.01 µM retinoic acid. Media was exchanged every 2 days.

Design and fabrication of MOA shape-pattering molds

Negative Polylactic acid (PLA) molds with convex, tubular features (1-5 mm in length, 0.8-1.5 mm in width, 1 mm in height) were designed in Autodesk Inventor Professional 2018 software and printed with an Ultimaker 3D printer. PDMS (Sylgard 184) and curing agent is mixed at 10:1 ratio and degassed in a desiccator for 1 hour. The mixture was poured onto the PLA mold and placed in an oven at 60 °C for 6 hours. After curation, PDMS containing arrays of concave wells was peeled from PLA and immersed in ethanol for 18 hours to remove uncured PDMS polymers. The PDMS mold was then autoclaved and immersed in an anti-cell adherence

solution (STEMCELL, Catalogue 07010) for 1 hour. After removal of the anti-adherence coating, PDMS molds were washed with PBS three times and to dry for use as a template for MOA shape pattering.

MOA patterning via molding

Day-12 organoids were harvested from Matrigel and centrifuged at 500 x *g* for 5 minutes (0°C). Supernatant was discarded and organoid pellet was resuspended with cold media (0°C), to remove residual Matrigel on the organoid surface. Organoids underwent a second centrifugation at 500 x *g* for 5 minutes (0°C) to form a compact pellet. Supernatant was removed and organoid pellet was carefully pipetted into the PDMS shape-patterning wells until the concave space was filled. To recreate mouse trachea anatomy (1-1.5 mm inner diameter), airway organoids were assembled within tubular wells of the same dimension (1-1.5 mm in width, 2-6 mm in length, 1 mm in height). MOAs were then overlaid with media and incubated in PDMS molds overnight to acquire the prescribed shape via contact guidance. Subsequently, MOAs were released from PDMS molds and cultured in a media-only condition in ultra-low attachment 6-well plates (Corning).

MOA formation via pipette extrusion

Day-12 organoids were harvested from Matrigel and centrifuged at 500 x *g* for 5 minutes (0°C). Supernatant was discarded and organoid pellet was resuspended with cold media (0°C), to remove residual Matrigel on the organoid surface. Organoids underwent a second centrifugation at 500 x *g* for 5 minutes (0°C) to form a compact pellet. Upon supernatant removal, organoid pellet was sucked into a 200 μL pipette tip and manually extruded into a string-like shape in warm media. The string-shaped aggregates were cultured long-term in a media-only, ultra-low attachment 6-well plate (Corning).

Image acquisition and analysis

Bright-field images of MOAs were acquired daily using an Olympus optical microscope with 4x and 10x objectives. The projected area of MOAs was measured using ImageJ software. For AIMR (= MOA area/inner matter area) quantification, optical images were corrected with background subtraction and converted into binary masks using the threshold function in ImageJ.

Time-lapse imaging was acquired by using a confocal spinning-disk microscope system (Intelligent Imaging

Innovations, Inc. 3i). The imaging system was composed of an Observer Z1 inverted microscope (Zeiss), a CSU X1 spinning disk head (Yokogawa), and a Quant EM 512SC camera (Photometrics). Silicon micro-inserts (4 well, Ibidi) were inserted into each well of an uncoated 8-well μ-slide (Ibidi). 8-12 Matrigel-depleted organoids were positioned within close proximity (less than 80 μm) in each mini-compartment created in the μ-slide. Organoids were grouped into three culture conditions: Floating, Gel-suspension (culture media supplemented with 20% volume fraction Matrigel in suspension) and the conventional Matrigel droplet culture. The μ-slide was mounted in a mini imaging compartment with controlled temperature (37 °C) and CO_2 concentration (5%). Organoid behaviours were recorded every 2 days with a 10x objective over a 10-day observation period. A x, y, z scanning mode was used to obtain z stack images. 3D image reconstruction and quantification of organoid dynamics (inter-organoid gap, envelope length, projected area of released inner matter) were performed in Slidebook6 software.

Immunofluorescent and histological staining

For immunofluorescent study, MOAs were prepared *via* pipette extrusion. MOAs at early-lumenization, mid-lumenization and stabilization stages were fixed with 4% paraformaldehyde (PFA) for 1 hour and washed three times with PBS under a fume hood. For immunofluorescent staining, fixed samples were permeabilized in 0.2% Triton X-100 in PBS for 1 hour, then blocked in 2% normal donkey serum (NDS) in PBS for 1 hour at room temperature. Primary antibodies (in 5% NDS/PBS solution at 1:200) were added and left overnight at 4°C, then washed off with 0.2% Tween-20 in PBS. Secondary antibodies were (in PBS at 1:2000) incubated for 1 hour at room temperature, then washed off with 0.2% Tween-20 in PBS. For staining DNA, DAPI (1:1000 dilution) was used for 5 minutes at room temperature. Antibodies are listed in the Additional Information.

For histological staining, fixed samples were embedded in paraffin wax and sectioned on a xyz microtome. Hematoxylin and eosin were used as dyes to stain respectively the cell nucleus (blue) and cytoplasm (pink).

Design and fabrication of a perfusable macro-organoid device

The millifluidics perfusion device was composed of a single-channel PDMS chip and a pair of pulled glass capillaries (1 mm outer diameter). A PLA template for the PDMS chip was designed in Autodesk inventor 2018 and printed with an Ultimaker 3D printer. A syringe needle (1 mm outer diameter) was assembled in the PLA

construct, before pouring the PDMS-curing agent mixture (10:1) into the PLA mold. After curing (60 °C, 6 hours), the needle was removed and PDMS was peeled from the PLA, followed by an immersion in ethanol for 18 hours. A 4 mm hole was punched in the centre of the PDMS chip, as a space to accommodate the macro-organoid tube. The PDMS chip was then bonded with a thin glass slide using a plasma cleaner (Harrick plasma) and autoclaved before use.

A macro-organoid tube was placed in the central culture area and Matrigel was added to fill the remaining culture space. The chip was incubated for 15 minutes to allow Matrigel gelation, followed by a top-up of the media reservoir with warm media. The airway-on-a-chip was stabilized in the incubator for at least 6 hours before mounted on an Olympus SZX16 upright optical microscope. Two glass capillaries were prepared using a micropipette puller (Sutter Instrument) and cut into 50 μm tip diameter with a micro forge (Narishige). Capillaries were autoclaved and pre-filled with culture media before insertion through the two ports of the PDMS chip. The inlet and outlet capillaries were connected to a Fisherbrand peristaltic pump through a media pre-filled silicone tubing, and carefully advanced toward the macro-organoid tube to cannulate the lumen. Direction and velocity of the media flow were tuned by controlling the rotating direction (clockwise or anti-clockwise) and speed (level 1 to 10) of the rotors. Flow rate calibration was performed prior to perfusion by recording the weight change of media droplets flowing from the silicone tubing.

Engineered co-culture of SMCs and macro-organoid tubes

Mouse vascular aortic smooth muscle cells MOVAS (ATCC® CRL-2797) were purchased from ATCC and cultured in DMEM (DB) supplemented with 10% FBS and antibiotics. To form SMC sheets, SMCs were passaged on 80% confluence and incubated in a temperature-responsive Nunc™ Dishe with UpCell™ Surface (ThermoFisher). When cells reached confluence, the UpCell plate was transferred to room temperature (20°C) to initiate temperature-regulated cell sheet detachment. SMC medium was discarded, and a macro-organoid tube was placed atop of a SMC sheet. Subsequently, the SMC sheet was careful lifted from the well bottom using forceps and wrapped around the macro-organoid tube, to create the co-culture construct. Organoid media was then added to the assembled tissue, which was cultured for 5 days before antibody staining.

Statistical analysis

All statistical analyses were performed in OriginLab 2015 software. *P* values were calculated using two-tailed Student's t-test and Mann-Whitney U test. *P*-values less than 0.05 were considered statistically significant. All box plots extend from the 25th to 75th percentiles, with a line at the median and whiskers extending to maximum and minimum data points. Each experiment was repeated at least twice using independent batches of organoids.

Acknowledgements

We thank Prof. Kim Dora, from Department of Pharmacology, University of Oxford for advice on vessel perfusion; Mr Lukas Vasadi, from Department of Engineering, University of Cambridge, for technical supports on the perfusion set-up. This work was supported by the European Research Council (ERC-StG, 758865; ERC-StG, 679411) and the Wellcome and the Royal Society (107633/Z/15/Z). Y. L. was a recipient of Schlumberger Faculty for the Future scholarship and Trinity Henry-Barlow scholarship. C.D. was supported by the Cancer Research UK Cambridge Centre PhD Studentship.

Author contributions

Y.L., J-H.L. and Y.Y.S.H. conceived and designed experiments. Y.L. conducted organoid fusion, perfusion, co-culture and analyzed data. B.S. performed live-cell imaging. C.D. and A.M. designed experiments, established organoids, conducted organoid fusion and staining, and analyzed biological characterizations. F.M. and E.T. did theoretical modelling. K.O., J-H.L. and Y.Y.S.H. assisted with results interpretation and figure design. Y.L., Y.Y.S.H., J-H.L., B.S. and E.T. wrote the manuscript.

Competing interest

The authors declare that they have no competing interests.

Data and materials availability

Extended data and materials, image processing code in the main text and supplementary information are available upon request by contacting the corresponding author.

References

1. Jakab, K., Neagu, A., Mironov, V., Markwald, R. R. & Forgacs, G. Engineering biological structures of prescribed shape using self-assembling multicellular systems. *Proc. Natl. Acad. Sci. U. S. A.* **101**, 2864–2869 (2004).
2. Murphy, S. V & Atala, A. 3D bioprinting of tissues and organs. *Nat Biotech* **32**, 773–785 (2014).
3. Skylar-Scott, M. A. *et al.* Biomanufacturing of organ-specific tissues with high cellular density and embedded vascular channels. *Sci. Adv.* **5**, eaaw2459 (2019).
4. Mironov, V. *et al.* Organ printing: Tissue spheroids as building blocks. *Biomaterials* **30**, 2164–2174 (2009).
5. Rago, A. P., Dean, D. M. & Morgan, J. R. Controlling cell position in complex heterotypic 3D microtissues by tissue fusion. *Biotechnol. Bioeng.* **102**, 1231–1241 (2009).
6. Tsai, A.-C., Liu, Y., Yuan, X. & Ma, T. Compaction, fusion, and functional activation of three-dimensional human mesenchymal stem cell aggregate. *Tissue Eng. Part A* **21**, 1705–1719 (2015).
7. Belair, D. G. *et al.* Engineering human cell spheroids to model embryonic tissue fusion in vitro. *PLoS One* **12**, e0184155 (2017).
8. Takeoka, Y. *et al.* Regeneration of esophagus using a scaffold-free biomimetic structure created with bio-three-dimensional printing. *PLoS One* **14**, e0211339 (2019).
9. Ayan, B. *et al.* Aspiration-assisted bioprinting for precise positioning of biologics. *Sci. Adv.* **6**, eaaw5111 (2020).
10. Sato, T. *et al.* Single Lgr5 stem cells build crypt-villus structures in vitro without a mesenchymal niche. *Nature* **459**, 262–5 (2009).
11. McCracken, K. W. *et al.* Modelling human development and disease in pluripotent stem-cell-derived gastric organoids. *Nature* **516**, 400–404 (2014).

12. Fujii, M. & Sato, T. Somatic cell-derived organoids as prototypes of human epithelial tissues and diseases. *Nat. Mater.* (2020) doi:10.1038/s41563-020-0754-0.
13. Brassard, J. A. & Lutolf, M. P. Engineering Stem Cell Self-organization to Build Better Organoids. *Cell Stem Cell* **24**, 860–876 (2019).
14. Takebe, T. & Wells, J. M. Organoids by design. *Science (80-.).* **364**, 956 LP – 959 (2019).
15. Xiang, Y. *et al.* Fusion of Regionally Specified hPSC-Derived Organoids Models Human Brain Development and Interneuron Migration. *Cell Stem Cell* **21**, 383-398.e7 (2017).
16. Bagley, J. A., Reumann, D., Bian, S., Lévi-Strauss, J. & Knoblich, J. A. Fused cerebral organoids model interactions between brain regions. *Nat. Methods* **14**, 743 (2017).
17. Sachs, N., Tsukamoto, Y., Kujala, P., Peters, P. J. & Clevers, H. Intestinal epithelial organoids fuse to form self-organizing tubes in floating collagen gels. *Development* **144**, 1107 LP – 1112 (2017).
18. Rock, J. R. *et al.* Basal cells as stem cells of the mouse trachea and human airway epithelium. *Proc. Natl. Acad. Sci.* **106**, 12771 LP – 12775 (2009).
19. Sebrell, T. A. *et al.* Live imaging analysis of human gastric epithelial spheroids reveals spontaneous rupture, rotation and fusion events. *Cell Tissue Res.* **371**, 293–307 (2018).
20. Chan, C. J. *et al.* Hydraulic control of mammalian embryo size and cell fate. *Nature* **571**, 112–116 (2019).
21. Wyatt, T. P. J. *et al.* Actomyosin controls planarity and folding of epithelia in response to compression. *Nat. Mater.* **19**, 109–117 (2020).
22. Doi, M. *Soft matter physics*. (Oxford University Press, 2013).
23. Simson, R. *et al.* Membrane bending modulus and adhesion energy of wild-type and mutant cells of Dictyostelium lacking talin or cortexillins. *Biophys. J.* **74**, 514–522 (1998).
24. Sackmann, E. & Bruinsma, R. F. Cell Adhesion as Wetting Transition? *ChemPhysChem* **3**, 262–269 (2002).
25. Co, J. Y. *et al.* Controlling Epithelial Polarity: A Human Enteroid Model for Host-Pathogen Interactions. *Cell Rep.* **26**, 2509-2520.e4 (2019).
26. Huh, D. *et al.* Reconstituting Organ-Level Lung Functions on a Chip. *Science (80-.).* **328**, 1662 LP – 1668 (2010).

27. Orhon, I. *et al.* Primary-cilium-dependent autophagy controls epithelial cell volume in response to fluid flow. *Nat. Cell Biol.* **18**, 657–667 (2016).

28. Navarro, M., Ruberte, J. & Carretero, A. 6 - Respiratory apparatus. in (eds. Ruberte, J., Carretero, A. & Navarro, M. B. T.-M. M. P.) 147–178 (Academic Press, 2017). doi:https://doi.org/10.1016/B978-0-12-812972-2.50006-4.

29. Park, S. E., Georgescu, A. & Huh, D. Organoids-on-a-chip. *Science (80-.).* **364**, 960 LP – 965 (2019).

30. Tysoe, O. C. *et al.* Isolation and propagation of primary human cholangiocyte organoids for the generation of bioengineered biliary tissue. *Nat. Protoc.* **14**, 1884–1925 (2019).

31. Capeling, M. M. *et al.* Nonadhesive Alginate Hydrogels Support Growth of Pluripotent Stem Cell-Derived Intestinal Organoids. *Stem Cell Reports* **12**, 381–394 (2019).

32. Gjorevski, N. *et al.* Designer matrices for intestinal stem cell and organoid culture. *Nature* **539**, 560 (2016).

33. Brandenberg, N. *et al.* High-throughput automated organoid culture via stem-cell aggregation in microcavity arrays. *Nat. Biomed. Eng.* (2020) doi:10.1038/s41551-020-0565-2.

34. Palmer, M. A. & Nelson, C. M. Fusion of airways during avian lung development constitutes a novel mechanism for the formation of continuous lumena in multicellular epithelia. *Dev. Dyn.* **n/a**, (2020).

35. Gervais, L., Lebreton, G. & Casanova, J. The making of a fusion branch in the Drosophila trachea. *Dev. Biol.* **362**, 187–193 (2012).

36. Moreno, E., Basler, K. & Morata, G. Cells compete for Decapentaplegic survival factor to prevent apoptosis in Drosophila wing development. *Nature* **416**, 755 (2002).

37. Tucker, A. S. Salivary gland development. *Semin. Cell Dev. Biol.* **18**, 237–244 (2007).

38. Sutherland, D., Samakovlis, C. & Krasnow, M. A. branchless Encodes a Drosophila FGF Homolog That Controls Tracheal Cell Migration and the Pattern of Branching. *Cell* **87**, 1091–1101 (1996).

39. Debnath, J. *et al.* The Role of Apoptosis in Creating and Maintaining Luminal Space within Normal and Oncogene-Expressing Mammary Acini. *Cell* **111**, 29–40 (2002).

40. Reid, J. A., Mollica, P. A., Bruno, R. D. & Sachs, P. C. Consistent and reproducible cultures of large-scale 3D mammary epithelial structures using an accessible bioprinting platform. *Breast Cancer Res.* **20**, 122 (2018).

41. Lee, J.-H. *et al.* Anatomically and Functionally Distinct Lung Mesenchymal Populations Marked by Lgr5 and Lgr6. *Cell* **170**, 1149-1163.e12 (2017).
42. Timoshenko, S. P. & Woinowsky-Krieger, S. *Theory of plates and shells*. (McGraw-hill, 1959).
43. Manibog, K., Li, H., Rakshit, S. & Sivasankar, S. Resolving the molecular mechanism of cadherin catch bond formation. *Nat. Commun.* **5**, 3941 (2014).
44. Charras, G. & Yap, A. S. Tensile Forces and Mechanotransduction at Cell-Cell Junctions. *Curr. Biol.* **28**, R445–R457 (2018).
45. Bell, S., Redmann, A.-L. & Terentjev, E. M. Universal Kinetics of the Onset of Cell Spreading on Substrates of Different Stiffness. *Biophys. J.* **116**, 551–559 (2019).
46. Cuvelier, D. *et al.* The Universal Dynamics of Cell Spreading. *Curr. Biol.* **17**, 694–699 (2007).

Figures

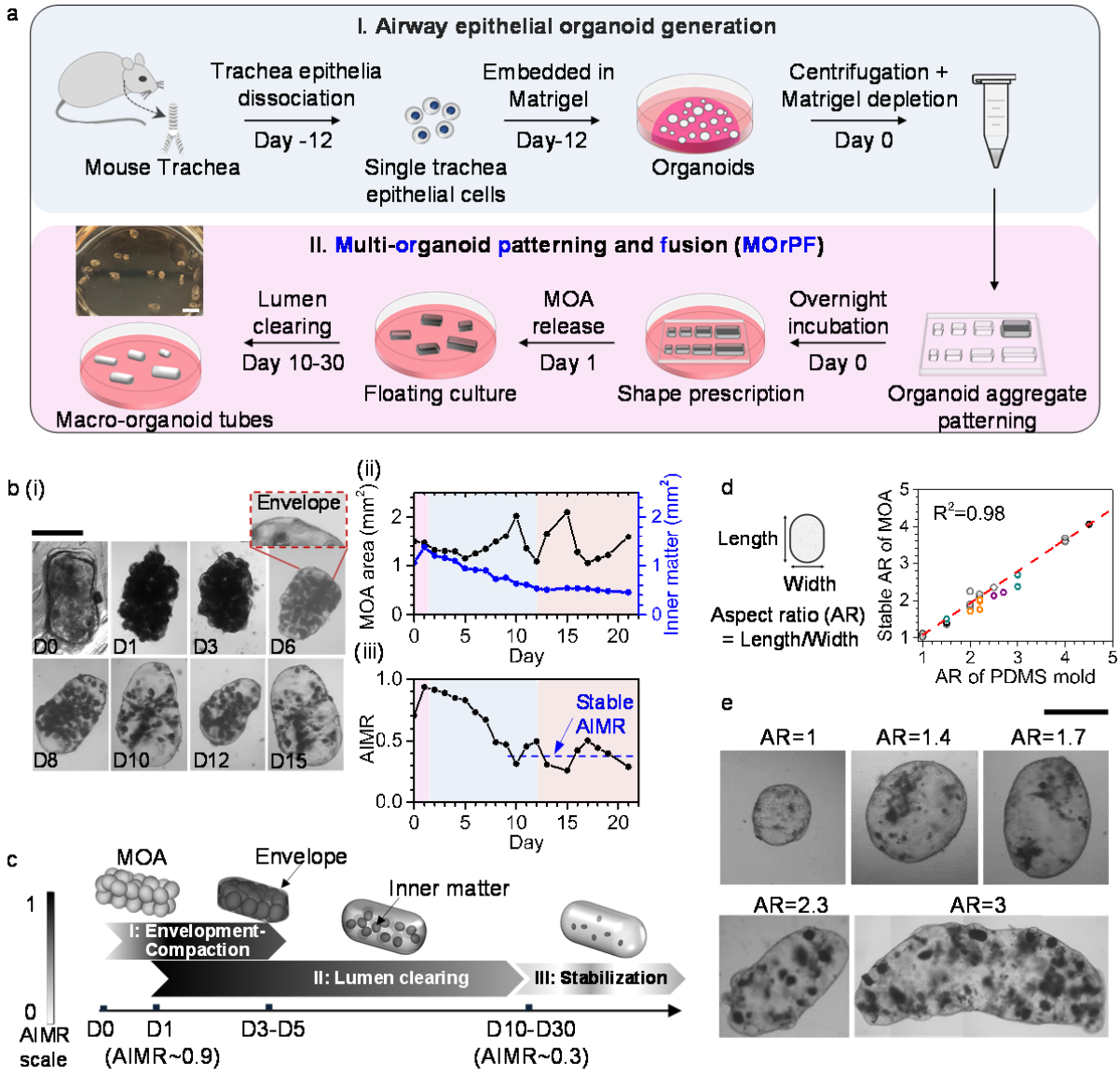

Fig. 1 | MOrPF technique guides the spatial assembly and fusion of airway organoids into upscaled, lumenized epithelial tubes. a, Schematic representation of mouse airway epithelial organoid generation (I), and the MOrPF procedure (II). Scale bar, 4 mm. b, (i) Representative image sequences (4 independent experiments) of a developing MOA. The MOA was patterned in a PDMS well on Day 0 and released into the floating culture on Day 1. Scale bar, 1mm; (ii) Dynamics of MOA fusion represented by the projected MOA area (black curve) and the inner matter area (blue curve); (iii) quantification of AIMR dynamics, approximating into a three-stage

process. AIMR=MOA area/Inner matter area. c, Schematic representation of the three stages in MOA fusion. MOA grey value corresponds to the AIMR scale. d, Aspect ratio of stabilized MOAs as a function of their initial aspect ratio prescribed by the PDMS mold. n=26 samples, from 6 independent experiments (each represented with a different color symbol). e, Representative images (4 independent experiments) of engineered macro-organoid tubes with a range of sizes and shapes. Scale bar, 1 mm.

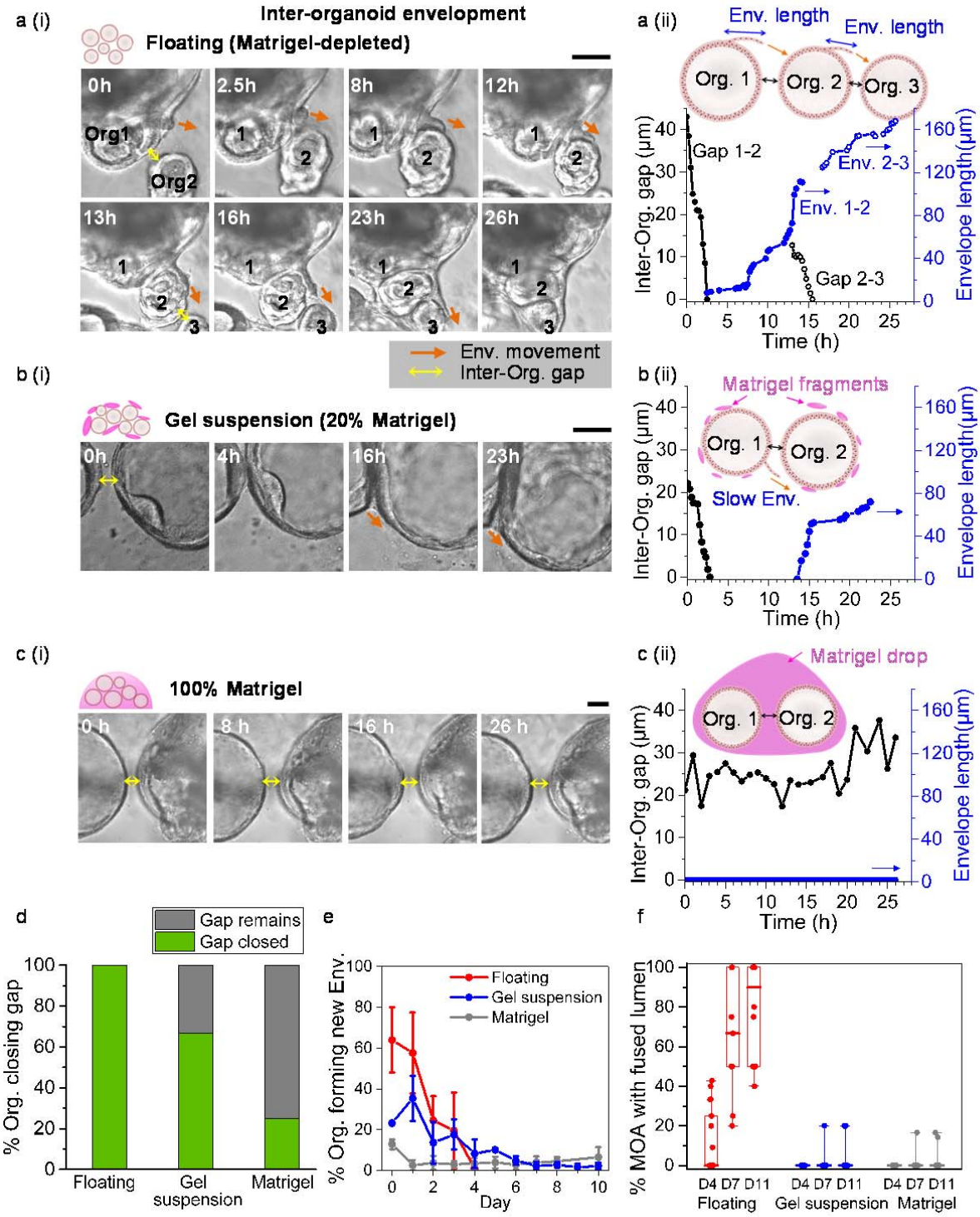

509

510 **Fig. 2** | Inter-organoid envelopment is a pre-requisite for MOA fusion. a-c, Live imaging and quantification of

511 inter-organoid envelope dynamics in Floating (a), Gel suspension (b) and full Matrigel (c) cultures. a(i), b(i),

512 c(i), Representative image sequences (3 independent experiments) highlighting changes in inter-organoid gaps

and the envelope leading edge positions for the three culture systems. Scale bars, 100 μm. a(ii), b(ii), c(ii), Measurement of inter-organoid gaps and envelope lengths for the corresponding organoids shown in the left panel. d, Percentage of organoids closing inter-organoid gaps (less than 80 μm) in the three culture systems. Floating, n=20; Gel suspension, n=15; Matrigel, n=20. e, Percentage of closely-spaced organoids developing new envelopes daily in the three cultures. Floating, n=193; Gel suspension, n=331; Matrigel, n=449. Data are presented as mean ± SD. f, Percentage of closely-spaced organoids undergoing successful fusion (as marked by the formation of a continuous lumen) in different culture systems. Midline = median, box = 25th-75th percentiles, Whisker = min and max values. Floating, n=10; Gel suspension, n=17; Matrigel, n=17.

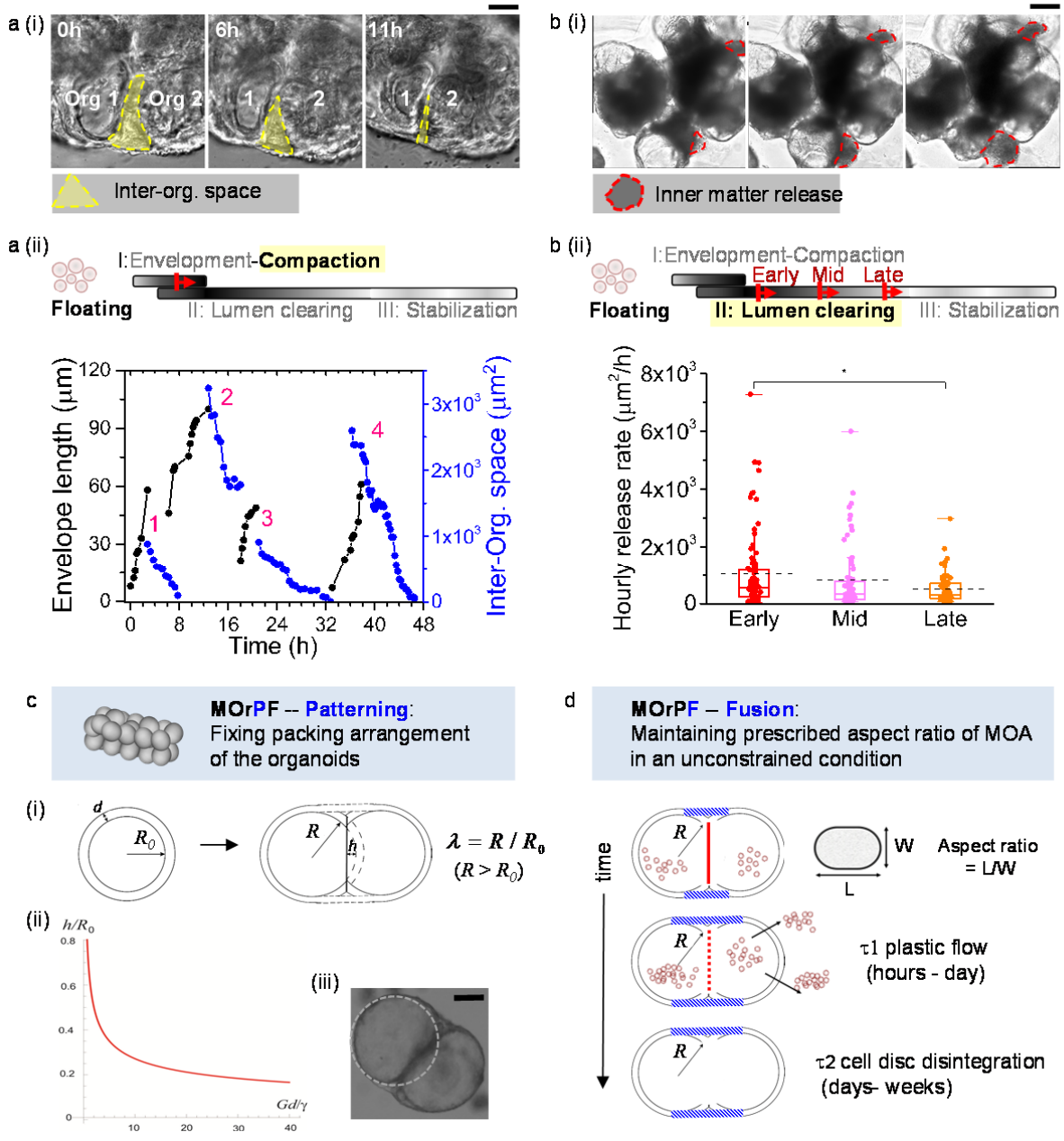

Fig. 3 | Dynamics of MOA compaction (a), inner matter release (b), and theoretical accounts for shape stability (c, d) in MOrPF. a(i), Representative image sequence (4 independent experiments) of MOA compaction via the closure of inter-organoid space. Scale bar, 100 μm. a(ii), Measurement of envelope length and the projected area of inter-organoid space over time. n=4 independent samples. Note that upon establishment, envelopes quickly integrated onto the organoid surfaces, with leading edges untrackable in the bright-field images. b(i), Representative image sequence (3 independent experiments) of MOA inner matter release. Scale bar, 500 μm. b(ii), Quantification of the released inner matter per hour in the Early, Mid and Late stages of MOA

lumenization. Early, n=79; Mid, n=68; Late, n=70. *P <0.05 by Mann-Whitney U test. c, Schematic representation of a physical model on MOA shape definition in the early stage of MOrPF. (i), Two organoids (radius R_0, shell thickness d) fuse to form a dumbbell-like structure consisting of two spherical caps with a larger radius $R > R_0$. h denotes how much the two organoids overlap to form the dumbbell. (ii) Theoretical model predicts the overlapping distance h/R_0 as a function of Gd/γ. (iii) Representative image (2 independent experiments) of two overlapping organoids joint by envelopes. Scale bar, 200 μm. d, Schematic representation of MOA shape maintenance in MOrPF. The dumbbell outer layer fluidizes in τ_1 (hours to days). After the disintegration of the adhesion disk in τ_2 (days to weeks), the new dumbbell shape will become the new quasi-equilibrium state, maintained by the high bending rigidity of the epithelial outer layer.

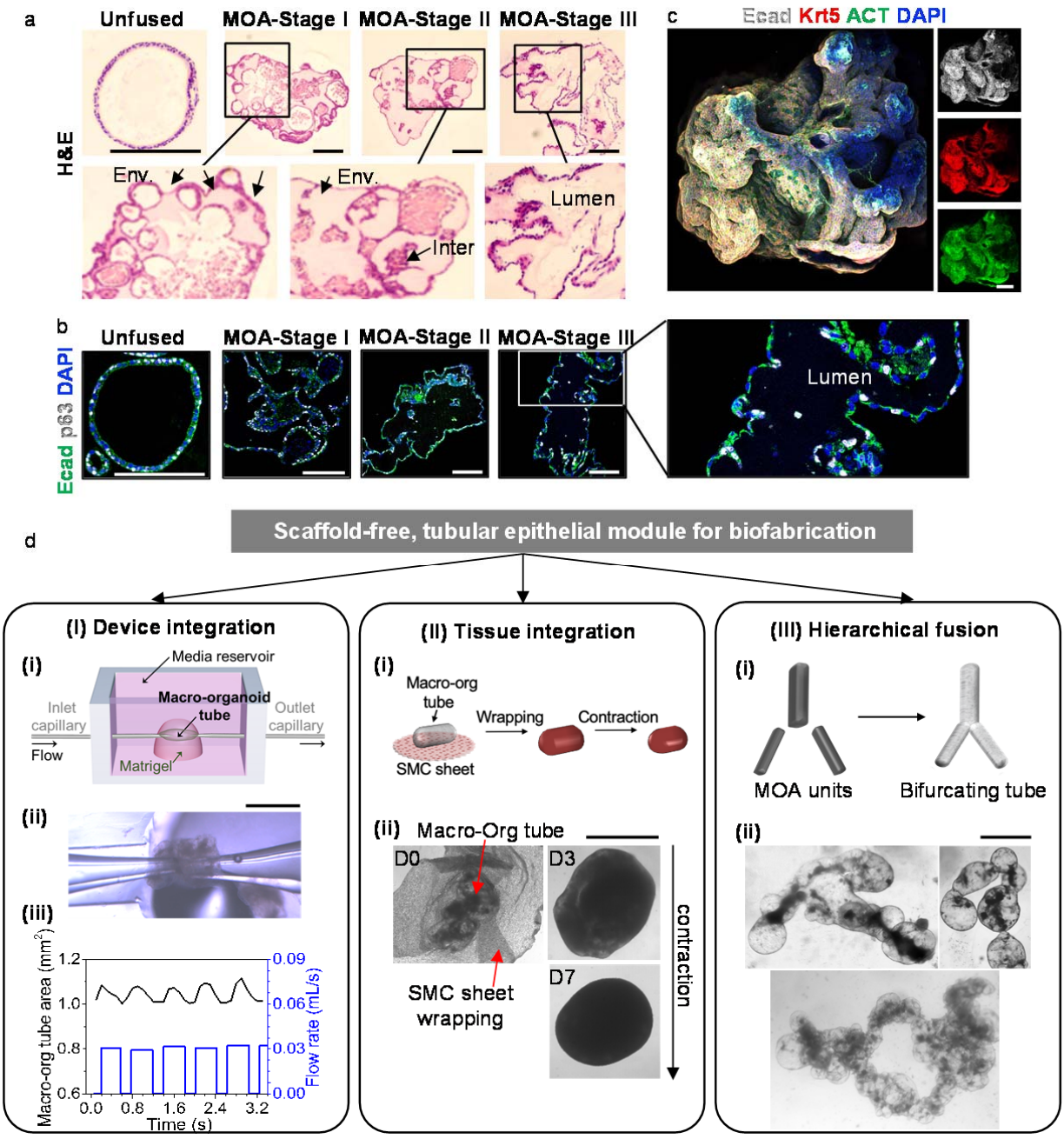

Fig. 4 | Biological characterization (a-c) and application (d) of bioengineered macro-organoid tubes. a, Representative H&E staining (three independent experiments) of an unfused airway organoid (control) and Stage I to III MOAs. Short arrows indicate 'envelope' structures whereas long arrows indicate the remaining 'interfacial' disks. Scale bar: 150 μm. b, Representative immunostaining (three independent experiments) of unfused airway organoids and Stage I to III MOAs for epithelial marker Ecad (green) and basal-cell marker p63 (white). Scale bar: 150 μm. c, 3D projection of a Stage II MOA, stained for nuclei (blue), Ecad (white), Krt5

(red) and ACT (green). Scale bar: 370 μm. d, Engineered macro-organoid tubes as scaffold-free building modules. **I.** Application in device-integration for a flow-able macro-organoid tube. (i) Two pulled glass pipettes cannulate the macro-organoid tube and connect its lumen to an external perfusion pump. (ii) Representative image (3 independent experiments) of a macro-organoid tube under media perfusion. Scale bar, 1mm. (iii) Quantification of the macro-organoid lumen area (black curve) in response to a peristaltic input flow (blue curve). **II.** Application in tissue integration. (i) Schematic representation of the macro-organoid-SMC co-culture procedure to form an integral tissue construct mimicking the mouse trachea. (ii) Representative images (3 independent experiments) of the co-culture. Scale bar, 1mm. **III.** Biofabrication via hierarchical MOA fusion. (i) Schematic representation of the assembly and fusion of MOA building blocks, to reconstitute typical hieratical architecture of branched tubular organs. (ii) Representative images (3 independent experiments) of engineered bifurcating epithelial macro-tubes. Scale bars, 1mm.